Colloids and Surfaces A: Physicochem. Eng. Aspects 499 (2016) 141–149

Contents lists available at ScienceDirect

Colloids and Surfaces A: Physicochemical and Engineering Aspects

journal homepage: www.elsevier.com/locate/colsurfa

Removal of Cu(II) ions from aqueous water by L-arginine modifying magnetic chitosan

Zhan-Chao Wu, Zhao-Zhan Wang, Jie Liu*, Jin-Hua Yin, Shao-Ping Kuang*

State Key Laboratory Base of Eco-Chemical Engineering, Laboratory of Inorganic Synthesis and Applied Chemistry, College of Chemistry and Molecular Engineering, Qingdao University of Science and Technology, Qingdao 266042, P.R. China

HIGHLIGHTS

- A novel magnetic chitosan modified by L-arginine was synthesized.
- The adsorption capacity and equilibrium time for Cu(II) were 2.13 mmol g^{-1} and 13 min, respectively.
- The adsorbent was easily separated from aqueous solution in 2 min by external magnetic field.
- The adsorbent exhibited good adsorption performance after five regeneration cycles.

GRAPHICAL ABSTRACT

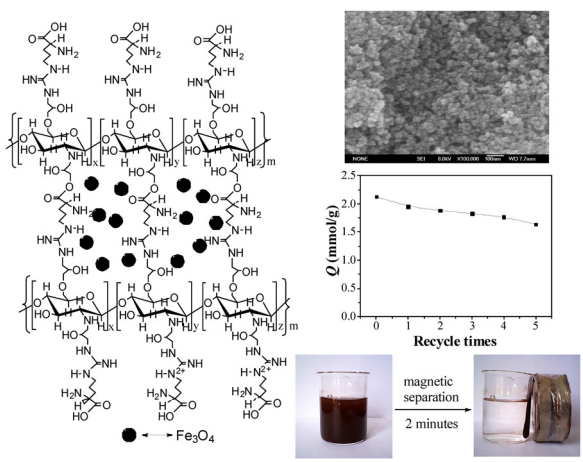

ARTICLE INFO

Article history:
Received 27 October 2015
Received in revised form 17 March 2016
Accepted 3 April 2016
Available online 6 April 2016

Keywords:
Magnetic chitosan
L-Arginine
Adsorption
Cu(II)

ABSTRACT

A new adsorbent L-Arg-CS/Fe_3O_4 was prepared by L-arginine modifying magnetic chitosan for the removal of Cu(II) ions from aqueous solution. The compositions of L-Arg-CS/Fe_3O_4 were characterized by infrared (IR) spectroscopy, X-ray diffraction (XRD) analysis and thermogravimetric (TG) analysis, respectively. The surface morphology, particle size and specific surface area were measured on scanning electron microscope (SEM) and micromeritics gas adsorption surface analyzer. The adsorption behavior of L-Arg-CS/Fe_3O_4 for Cu(II) were investigated as a function of pH, contact time and initial Cu(II) concentration. The maximum adsorption capacity for Cu(II) was 2.13 mmol g^{-1} at the optimized adsorption conditions, which were pH = 5.5, t = 13 min, C_0 = 4.0 mmol L^{-1}. The adsorption behavior was evaluated by the analysis of adsorption kinetics. Freundlich and Langmuir isotherm models were used to estimate the adsorption mode. L-Arg-CS/Fe_3O_4 exhibited high adsorption capability after five regeneration cycles. The adsorption and desorption mechanisms were discussed. The results show that L-Arg-CS/Fe_3O_4 is a promising adsorbent for removal of Cu(II) from aqueous solutions.

1. Introduction

At present, wastewater containing heavy metal ions is one of serious environmental problems and has attracted global attention because of their high toxicity and non-biodegradability [1–3]. Trace

* Corresponding author.
E-mail addresses: zsuliujie@163.com (J. Liu), qustksp@126.com (S.-P. Kuang).

http://dx.doi.org/10.1016/j.colsurfa.2016.04.012
0927-7757/

amounts of heavy metal ions can cause serious pollution problem. Among these heavy metals, copper is commonly used one, which is abundant in waste streams from copper electroplating and textile industries. Copper is one of the elements which is essential for human beings, but at higher concentration it affects the health of fauna, flora and humans adversely. The excess intake of copper by the human body may lead to severe mucosal irritation, capillary damage, renal damage, liver and kidney damage, stomach and intestinal irritation, and anemia [4,5]. In addition, excess copper in marine systems has been found to damage marine life, primarily damaging the gills, liver, kidneys, and nervous system, as well as changing the sexual life of fishes [6]. So the removal of copper from wastewater is one of the most significant subjects [7,8].

Nowadays, the adsorption technique using choitosan (CS) as adsorbent has become research hotspot for removing Cu(II) from wastewater due to the advantages of easy operation, low cost and no secondary pollution [9–14]. This technique is superior to other processes, such as chemical precipitation, ion exchange and electrochemical separation process. CS molecules are rich in amino and hydroxyl groups, which show high reaction activity with heavy metal ions. Therefore, CS can be used as heavy metal ions adsorbent [15,16]. However, the adsorption capacity of CS is still insufficient owing to the limited adsorption sites. This limits its application in the practical treatment of heavy metal ions [17,18]. It is necessary for modifying CS in order to improve adsorption performance. Generally, modifiers with high content of nitrogen, oxygen or sulfur are preferred to improve adsorption capability of CS, such as triethylene-tetramine (TETA) [19], ethanediamine [20], melamine[21], thiol [22–24], and ethylenediaminetetraacetic acid (EDTA) [25].

L-Arginine (L-Arg) molecule possesses several amino groups and a carboxyl, which show strong coordination capability with Cu(II) [26,27]. So, it is expected to obtain high efficient and low cost adsorbent by grafting L-Arg onto CS. However, CS modified by L-Arg as adsorbent has rarely been reported as far as we know.

Moreover, how to separate adsorbents from aqueous solution thoroughly is another important matter in order to avoid secondary pollution. Traditional separation methods are both time-consuming and uneconomic, such as filtration, sedimentation and centrifugation [28,29]. Therefore, it is necessary to choose a rapid and effective separation method. Magnetic separation technology meets this need nicely and has been used in separating adsorbents from aqueous solution [30–33]. Large amounts of adsorbents can be separated from aqueous solution in a very short time costing less energy and producing no pollutant.

In this work, a new material (magnetic CS modified by L-Arg, L-Arg-CS/Fe_3O_4) for Cu(II) adsorption was synthesized successfully. The adsorption capacity of L-Arg-CS/Fe_3O_4 was optimized by varying initial pH, adsorption time and initial Cu(II) concentration. The adsorption behaviors were investigated by simulating the adsorption kinetics curve and adsorption isotherm.

2. Experimental

2.1. Materials

CS (deacetylation rate > 90%) was purchased from Lanji technology development Co., Ltd. (Shanghai, China). Epoxy chloropropane was obtained from Sinopharm Chemical Reagent Co., Ltd. (Shanghai, China). L-Arg was obtained from Bodi chemical engineering Co., Ltd. (Tianjin, China). Fe_3O_4 with purity of 99.5% was purchased from Aladdin Chemistry Co., Ltd (Shanghai, China). Solutions of Cu(II) were prepared by dissolving appropriate $CuSO_4{\cdot}5H_2O$ (Hongyan chemical reagent factory, Tianjin, China) in deionized water. All other reagents are analytical grade and used without further purification. Deionized water was used in the preparation of all solutions.

2.2. Preparation of L-Agr-CS/Fe_3O_4

CS powders (1.00 g) were dissolved in acetic acid (2% wt, 100 mL) and stirred for 20 min. The mixtures were dropped into NaOH (0.25 mol L^{-1}, 100 mL) under stirring. After precipitation, the mixtures were filtered and the precipitation was washed with acetone. The residues were transferred to acetone (100 mL) and stirred until to suspensions. Epoxy chloropropane (5 mL) was added to above suspensions. Then the mixtures were stirred continuously at 298 K for 24 h. After that, Fe_3O_4 (0.75 g) was added and ultrasonic dispersion was implemented for 20 min. Solid and liquid were separated by suction filtration. The filter case was added in acetone (60 mL). Next, L-Arg (2.00 g) dissolved in deionized water (40 mL) was added into above solution system and reflux was continuous for 7 h at 333 K. Following this, L-Arg (0.25 g) dissolved in deionized water (10 mL), NaOH (1.00 mol L^{-1}, 30 mL) and KI (0.05 g) were added in sequence, and the mixtures were stirred for 5 h. Then the products were cooled, separated from solution by magnet and washed with deionized water and acetone orderly. Finally, the residues were dried in vacuum drying oven at 333 K.

The schematic diagram of synthesis route is illustrated in Fig. 1.

2.3. Adsorption experiments

Appropriate amounts of L-Arg-CS/Fe_3O_4 were added into Cu(II) solution (20 mL). After adjusting the pH values, the mixtures were shaken in shaker under the designed conditions. Then, the adsorbents were separated from solutions by external magnet. Residual concentration of Cu(II) was measured on flame graphite furnace atomic absorption spectrophotometer (AAS, 6810F/6810GF). The amounts of Cu(II) adsorbed by per unit mass of adsorbent were obtained by the following equation:

$$Q = \frac{(C_0 - C_e)}{m} V \quad (1)$$

where Q is the adsorption capacity of adsorbent for Cu(II) (mmol g^{-1}); C_0 is the initial concentration of Cu(II) (mmol L^{-1}); C_e is the equilibrium concentrations of Cu(II) (mmol L^{-1}); V and m are the volume of solution (L) and the mass of the dry adsorbent (g).

2.3.1. Effect of pH

Six solution systems with Cu(II) ions (4 mmol L^{-1}) were prepared by adjusting initial pH = 1.0, 2.0, 3.0, 4.0, 5.0 and 5.5. The pH values of the solutions were measured on pH meter (PHS-25C, Aolilong, Hongzhou). The adsorption experiments were performed by shaking L-Arg-CS/Fe_3O_4 adsorbent (10 mg) with different solution systems (20 mL) for 13 min. The residual Cu(II) concentration in upper clear liquid was detected by AAS.

2.3.2. Effect of contact time

The removals of Cu(II) at different time intervals were performed by shaking L-Arg-CS/Fe_3O_4 adsorbents (10 mg) with Cu(II) solutions (4 mmol·L^{-1}, 20 mL, pH = 5.5). Ten parallel experiments were done according to different adsorption time of 1, 3, 5, 7, 9, 11, 13, 15 min. The residual Cu(II) concentration was measured on AAS.

2.3.3. Effect of initial concentration

Ten solution systems (pH = 5.5) were prepared by varying Cu(II) initial concentrations. The initial concentrations of Cu(II) ions were 0.25, 0.5, 1.0, 2.0, 3.0, 4.0, 5.0, 6.0, 7.0 and 8.0 mmol L^{-1}, respectively. The adsorption tests in different solutions were handled

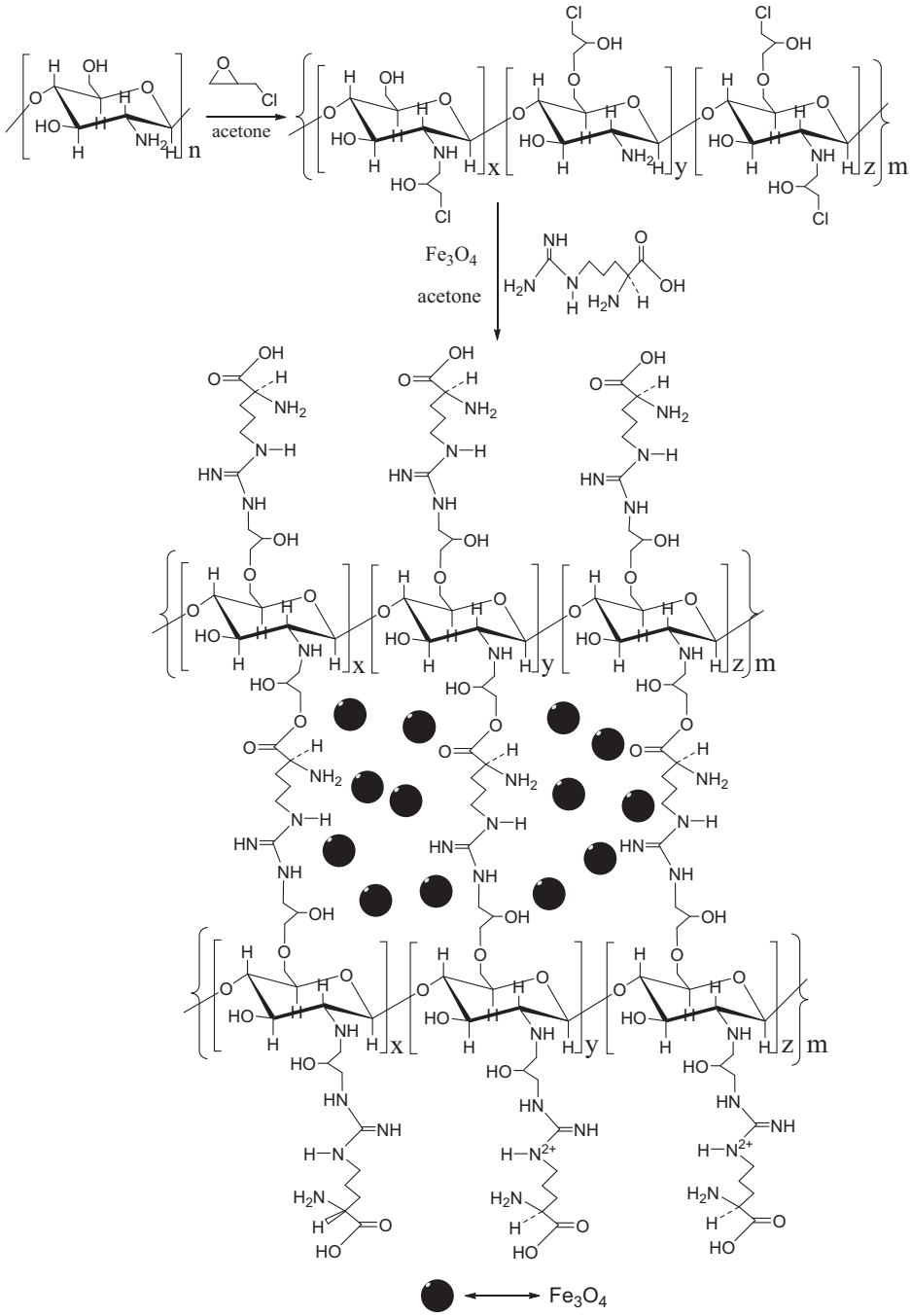

Fig. 1. Synthesis route of L-Arg-CS/Fe_3O_4.

under shaking for 13 min. After magnetic separation, the residual Cu(II) concentration in solution was measured by AAS.

2.4. Desorption and regeneration studies

The adsorbents loading with Cu(II) were collected and washed fully with deionized water. Then, they were placed into HCl solutions (0.5 mol L^{-1}) and shaken continuously for 2 h. After desorption and separation, the adsorbents were washed with deionized water again. The above operations were repeated until no Cu(II) ions were detected in washing liquid. Then they were soaked in NaOH solution (0.5 mol L^{-1}) under stirring for 2 h. After magnetic separation, the adsorbents were washed by deionized water and acetone orderly. Finally, they were dried in vacuum drying oven at 333 K. After completing the above steps, the adsorbents were regenerated.

The adsorption and desorption processes were repeated for five times.

2.5. Characterization of the samples

Infrared (IR) spectra were carried out on FT-IR spectrometer (Nicolet 510P, Nicolet, America). X-Ray diffraction (XRD) patterns were recorded on X-ray diffractometer (D-MAX 2500/PC, Rigaku, Japan) at voltage of 40 kV and current of 50 mA. The scanning scope of 2-theta was from 5° to 80°. The samples morphologies were observed on cold field emission scanning electron microscope (SEM) (JSM-6700F, Hitachi, Japan). The surface area

Table 1
Comparison of adsorption performances of different adsorbents for Cu(II) ions.

Adsorbent	Equilibrium time (min)	Adsorption capacity (mg g^{-1})	Reference
Raw Chitosan	60	80.17 mg g^{-1}	[34]
Magnetic chitosan microspheres	250	66.70 mg g^{-1}	[35]
Magnetic Cu(II) ion imprinted composite	360	71.36 mg g^{-1}	[36]
Epichlorohydrin cross-linked xanthate chitosan	1440	30.21 mg g^{-1}	[37]
Xanthate-modified magnetic chitosan	–	26.3 mg g^{-1}	[38]
chitosan-modified magnetic Mn ferritenanoparticles	500	65.1 mg g^{-1}	[31]
S-doped Fe_3O_4@C NPs	>300	54.7 mg g^{-1}	[39]
L-Arg-CS/Fe_3O_4	13	135.3 mg g^{-1}	This work
L-Arg-CS (calculated)	–	201.3 mg g^{-1}	This work

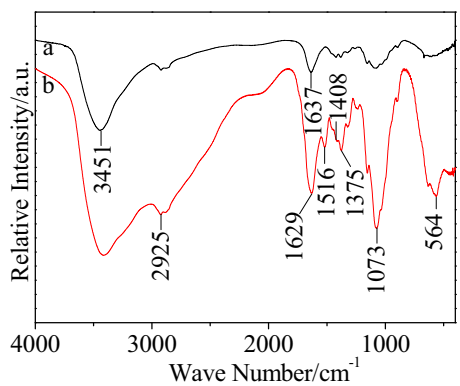

Fig. 2. IR spectra of CS (a) and L-Arg-CS/Fe_3O_4 (b).

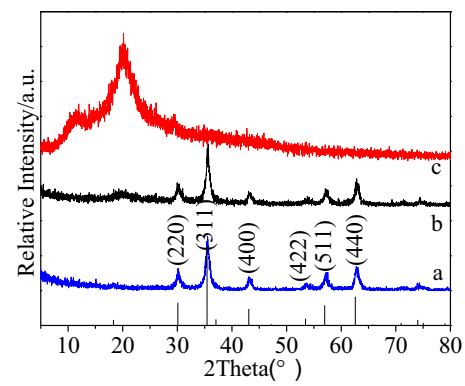

Fig. 3. XRD patterns of Fe_3O_4 (a), L-Arg-CS/Fe_3O_4 (b) and CS (c).

were measured on micromeritics gas adsorption surface analyzer (ASAP 2020, Micromeritics, America). The content of each component in L-Arg-CS/Fe_3O_4 was determined by thermogravimetric (TG) and differential scanning calorimetric (DSC) analysis. The measurement was performed on simultaneous thermal analyzer (STA449C, NETZSCH, Germany) under dynamic nitrogen flow with 50 cm^3 min^{-1} flow velocity and the heating rate is 10 K min^{-1}. The point of zero charge and different Zeta Potential values of the L-Arg-CS/Fe_3O_4 were measured on nano-particle diameter potential analyzer (Nano-ZS90, Malvern, UK).

3. Results and discussion

3.1. Characterization

3.1.1. IR spectra analysis

Fig. 2 shows the IR spectra of CS (curve a) and L-Arg-CS/Fe_3O_4 (curve b). There are several functional groups in L-Arg molecular including —NH_2, —NH—, —COOH. As shown in Fig. 2, the difference between the IR spectrum of CS with that of L-Arg-CS/Fe_3O_4 is the appearance of peaks at 1629 and 1375 cm^{-1}. The two peaks are attributed to the asymmetry and symmetry stretching vibration of —COO— in L-Arg molecular. The reaction between —Cl (epichlorohydrin) and —NH_2 (L-Arg) was confirmed by the obviously strengthened peak at 1073 cm^{-1} in IR spectra of L-Arg-CS/Fe_3O_4, which is assigned to the stretching vibration of —C—N. In addition, the characteristic adsorption peak of Fe—O bond (564 cm^{-1}) appears in IR spectra of L-Arg-CS/Fe_3O_4. The characteristic peaks of the groups in both L-Arg and Fe_3O_4 were observed in IR spectra of L-Arg-CS/Fe_3O_4, implying that L-Arg-CS/Fe_3O_4 was prepared successfully.

3.1.2. XRD analysis

Fig. 3 presents the XRD patterns of Fe_3O_4 (curve a), L-Arg-CS/Fe_3O_4 (curve b) and CS (curve c). CS exhibited two characteristic peaks at about 2θ = 10° and 20°, respectively. But the two peaks were weakened in L-Arg-CS/Fe_3O_4 due to the introduction of epoxy chloropropane, L-Arg and Fe_3O_4. The diffraction peaks of Fe_3O_4 (2θ = 30.1°, 35.5°, 43.3°, 57.2° and 62.5°, JCPDS card No. 65-3107) were also observed in XRD pattern of L-Arg-CS/Fe_3O_4, indicating that Fe_3O_4 was introduced into the adsorbent successfully. The diffraction intensity of L-Arg-CS/Fe_3O_4 became weaker than that of CS and Fe_3O_4. All the XRD data suggest that L-Arg and Fe_3O_4 have been introduced into CS successfully.

Table 2
Estimated adsorption kinetic parameters for the adsorption of Cu(II) onto L-Arg-CS/Fe_3O_4.

First-Order			Second-Order			Intraparticle Diffusion		
Q_e	k_1	R^2	Q_e	k_2	R^2	K_P	C	R^2
2.15	0.4	0.98369	2.39	4.07	0.99909	−1.36	2.15	0.93705

3.1.3. SEM and BET surface area analysis

The SEM micrographs of L-Arg-CS/Fe_3O_4 are shown in Fig. 4. It can be seen that the particles are approximate spherical shape and the diameter size is about 20–25 nm. Slight agglomerate phenomenon was observed. The particles size is nanometer-scale, which mean that the adsorbents may have large specific surface area. So nitrogen adsorption measurements were used to determine the BET specific surface area of L-Arg-CS/Fe_3O_4. The BET specific surface area of L-Arg-CS/Fe_3O_4 is 54.83 m^2 g^{-1}. Large specific surface area is favorable for adsorption.

3.1.4. TG and DSC analysis

Fig. 5 reveals the TG and DSC curves of CS and L-Arg-CS/Fe_3O_4. For CS sample, the water loss process started at 20 °C and finished at 100 °C. The loss rate was almost about 0.0%. That is to say that there is almost no water in CS sample. The next was organic matter decomposition stage from 100 to 580 °C. The weight loss and enthalpy were about 89.8% and 3732.67 J g^{-1}, which corresponded to the decomposition of and heat release of CS, respectively. In this stage, the weight loss ratio was only 6.1% due to the partial decomposition of CS when temperature was up to 260 °C. The sample

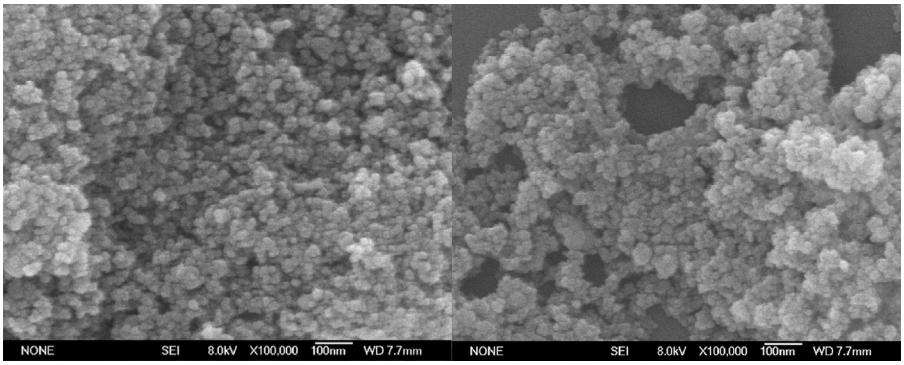

Fig. 4. SEM micrographs of L-Arg-CS/Fe_3O_4.

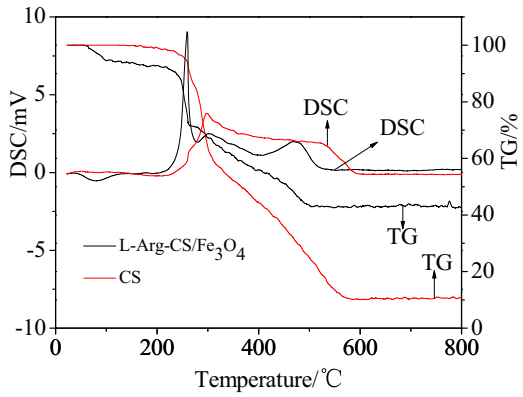

Fig. 5. TG and DSC curves of CS (red lines) and L-Arg-CS/Fe_3O_4 (black lines). (For interpretation of the references to colour in this figure legend, the reader is referred to the web version of this article.)

weight was almost unchanged from 580 to 800 °C. This was considered as the residual component after decomposition of CS. The residual weight was about 10.2%. Accordingly, the value of enthalpy change was almost zero, implying that there was almost no heat release in this stage. For L-Arg-CS/Fe_3O_4 sample, the weight loss was about 5.5% between 20 and 100 °C due to the volatilization of water. Compared to the curves of CS, it is not difficult to find that the decomposition of L-Arg occurred between 100 and 265 °C, and the weight loss was 22.9%. Correspondingly, a sharp and strong exothermic peak appeared in the DSC curve of L-Arg-CS/Fe_3O_4 sample, suggesting a strong exothermic process when the L-Arg was decomposed. Next, similar to the CS curve, it was the decomposition process of CS from 265 to 500 °C. The weight loss ratio is about 28.6%. After that, the weight of the sample was almost unchanged. Also, the enthalpy change value is almost zero. Since Fe_3O_4 could not be oxygenated under nitrogen atmosphere, the residues should be the decomposition residue of CS and Fe_3O_4. The residues weight ratio is about 42.9%. Combined with pure CS decomposition data, the mass content of L-Arg, CS and Fe_3O_4 in L-Arg-CS/Fe_3O_4 is estimated to be about 16.8%, 44.9% and 32.8%, respectively. Therefore, the weight ratio of H_2O: L-Arg: CS: Fe_3O_4 can be roughly estimated to be 5.5: 16.8: 44.9: 32.8. The decomposition temperature of L-Arg-CS/Fe_3O_4 was lower than that of pure CS, which also implies the changes of structure and chemical bonds after modification.

3.1.5. Magnetic separation performance

Fig. 6 illustrates separation behavior of L-Arg-CS/Fe_3O_4 under magnetic field. The nanometer-scale adsorbent was quickly separated from aqueous solution in 2 min. It is favorable to the recycle of the adsorbents.

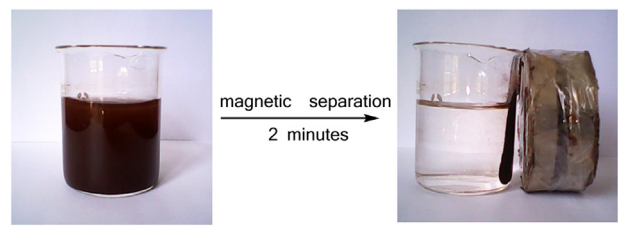

Fig. 6. The separation process of L-Arg-CS/Fe_3O_4 from the suspensions.

3.2. Influence of operating conditions on adsorption of Cu(II)

3.2.1. Effects of initial pH

Fig. 7 shows the effects of initial pH value on adsorption capacity of L-Arg-CS/Fe_3O_4. The equilibrium adsorption capacity increased with pH value increasing from 1.0 to 5.5. When pH value was higher than 4.0, the adsorption capacity increased markedly. This result may be explained by the following facts. There are large amounts of active groups, including amino, imino, carboxyl and hydroxyl on the surface of L-Arg-CS/Fe_3O_4. At low pH, high concentration of H^+ has higher mobility and stronger coordination ability as compared to metal ions so that lots of active groups on L-Arg-CS/Fe_3O_4 are easily protonated. Consequently, the electron-donating ability of N or O atoms are weakened, which is unfavorable to Cu(II) adsorption because of electrostatic repulsion. As the pH value increases, the adsorption capacity increases because the protonation are weaken but coordination effects are strengthened between L-Arg-CS/Fe_3O_4 and Cu(II). It is more suitable for adsorption between L-Arg-CS/Fe_3O_4 and Cu(II) at high pH value. In order to further illustrate the influence of pH value, the point of zero charge of L-Arg-CS/Fe_3O_4 was measured by nano-particle diameter potential analyzer. The pH value was confirmed to be about 3.5 at the point of zero charge of the L-Arg-CS/Fe_3O_4. The Zeta Potential of L-Arg-CS/Fe_3O_4 was negative when pH value was greater than 3.5. And the value became more negative with the increase of pH. In this case, it was favorable for the adsorption Cu(II) due to the electrostatic attraction. In contrast, the Zeta Potential became positive with the further decrease of pH value (pH < 3.5). Obviously, it is unfavorable for the adsorption Cu ions because of the electrostatic repulsion. This result is basically consistent with the previous analysis and further confirms the correctness of previous analysis. When pH value was over 5.5, $Cu(OH)_2$ precipitation was generated in Cu(II) solution. Therefore, the optimal pH value for Cu(II) adsorption was determined to be 5.5 and the saturated adsorption capacity was 2.03 mmol g^{-1} in this situation.

3.2.2. Adsorption kinetics

Fig. 8 shows the adsorption kinetic curve of Cu(II) ions on L-Arg-CS/Fe_3O_4. The adsorption quantity (Q) increased sharply at the

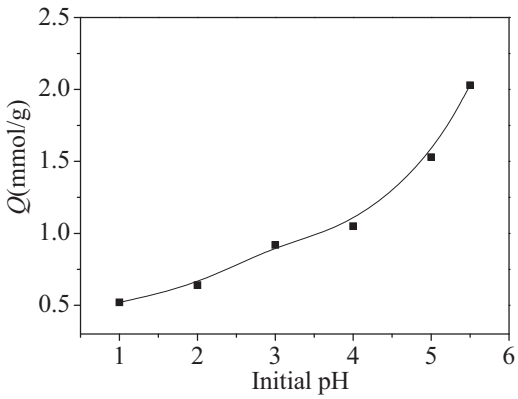

Fig. 7. Effects of initial pH value on adsorption capacity.

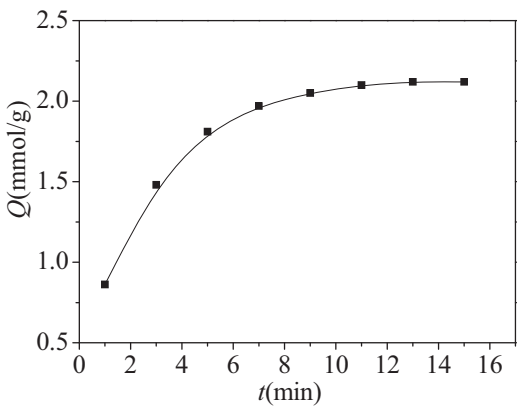

Fig. 8. Effects of contact time on adsorption capacity.

beginning, and then the increase speed slowed down gradually. Finally, it was close to adsorption equilibrium at 13 min. So the optimal adsorption time was confirmed to be 13 min, which was much shorter than those of the previously reported adsorbents (see Table 1) [31,34–39]. The saturated adsorption capacity was 2.12 mmol g^{-1}.

Pseudo-first-order and pseudo-second-order kinetic models were introduced in order to investigate the adsorption behavior of Cu(II) ions on L-Arg-CS/Fe_3O_4.

The pseudo-first-order equation [40] is expressed as follows.

$$\log(Q_e - Q_t) = \log(Q_e) - \frac{k_1 t}{2.303} \quad (2)$$

where Q_e and Q_t (mmol g^{-1}) are the adsorption quantities at equilibrium and unequilibrium time (min), respectively; k_1 is the rate constant of pseudo-first-order adsorption (min^{-1}); t is adsorption time (min). The slope and intercept of the plot of $\log(Q_e\text{-}Q_t)$ versus t are used to determine the first-order rate constant k_1. The slope and intercept are k_1/Q_e and $1/Q_e$, respectively (see Fig. 9a).

Table 3
Simulated adsorption isotherm parameters for the adsorption between Cu(II) and L-Arg-CS/Fe_3O_4.

Freundlich isotherm			Langmuir isotherm		
n	K_F(mmol/g)	R^2	Q_{max}(mmol/g)	K_L(g/mmol)	R^2
2.82	1.31	0.90866	2.25	3.11	0.99912

Another one is pseudo-second-order equation [41].

$$\frac{t}{Q_t} = \frac{1}{k_2 Q_e^2} + \frac{t}{Q_e} \quad (3)$$

where k_2 is the equilibrium rate constant of pseudo-second-order adsorption (g·mmol^{-1}·min^{-1}). The slope and intercept of plotting of t/Q_t versus t were used to calculate the second-order rate constant k_2. The slope and intercept are $1/Q_e$ and $1/K_2{Q_e}^2$, respectively (see Fig. 9b).

The relevant kinetic parameters obtained from eq. (2) and (3) are listed in Table 2. By comparison, it can be found the correlation coefficient (R^2) obtained from the second-order adsorption kinetic model (0.99909) is higher than that from the first-order kinetic model (0.98369), suggesting that the pseudo-second-order equation is more appropriate to simulate the experimental kinetic data [42]. The results indicate that the adsorption rate of Cu(II) ions on L-Arg-CS/Fe_3O_4 appears to be controlled by the chemical adsorption [43,44].

Most adsorption reactions contain several steps (i) external film diffusion, (ii) intra-particle diffusion and (iii) chemical adsorption. Since the first step is excluded by sufficient shaking the solution, the rate-controlling step is one of the latter two steps. So the data were treated by intra-particle diffusion model [45,46] in order to evaluate the contribution of intra-particle diffusion on rate-controlling step. Its equation is expressed as:

$$Q_t = k_p t^{1/2} + C \quad (4)$$

where k_p is the rate constant of the intra-particle diffusion (mmol g^{-1} $min^{1/2}$). The values of k_p and C were calculated via the slope and intercept of the plot of Q_t versus $t^{1/2}$ (see Fig. 10) and the results are also listed in Table 2. It is found the value of R^2 is low (0.93705), indicating the intra-particle diffusion model fits badly with the experimental data. Therefore, the rate-controlling step is not supposed to be intra-particle diffusion, but chemical adsorption. The result is in agreement with the kinetic results reported by Zhou et al. [44].

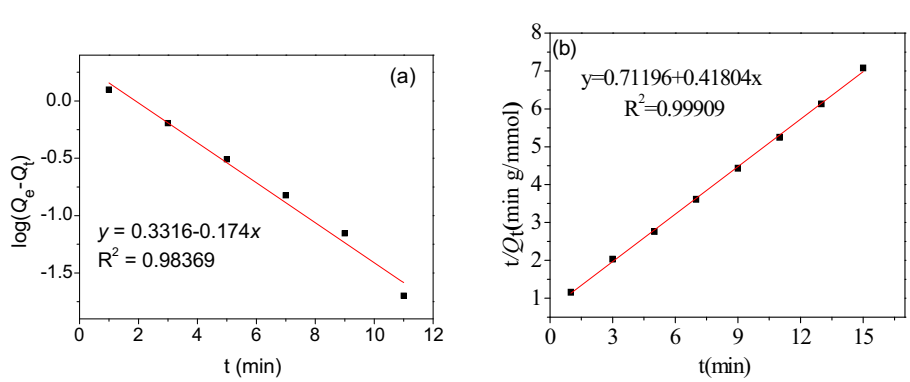

Fig. 9. The adsorption models of first-order kinetics (a) and second-order kinetics (b).

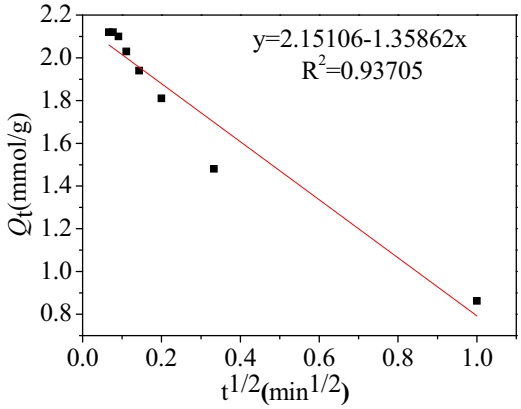

Fig. 10. The intra-particle diffusion model for Cu(II) adsorption by L-Arg-CS/Fe_3O_4.

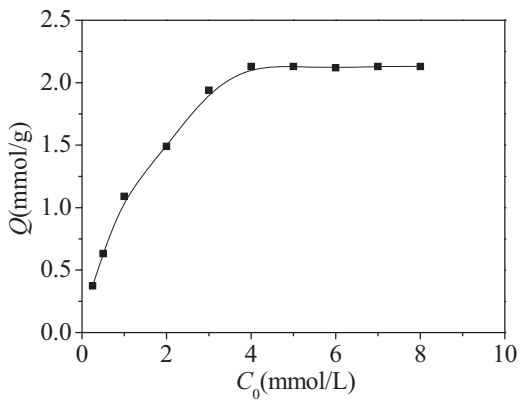

Fig. 11. Effects of initial Cu(II) concentrations on adsorption capacity.

3.2.3. Equilibrium adsorption isotherms

Fig. 11 shows the effects of initial Cu(II) concentrations on the adsorption capacity. At first, the adsorption capacity increased sharply with the increase of initial Cu(II) concentration. Then, the momentum slowed down. The adsorption capacity achieved maximum at C_0 = 4.0 mmol L^{-1}. After that, it remained unchanged. The maximum adsorption capacity was determined to be 2.13 mmol g^{-1} (135.3 mg g^{-1}). In fact, L-Arg-CS was the effective component for adsorption of Cu(II) ions. Fe_3O_4, which was encapsulated inside the adsorbent, showed little adsorption of Cu(II). However, the mass content of Fe_3O_4 in L-Arg-CS/Fe_3O_4 reached up to 32.8% according to the TG analysis. Therefore, the adsorption capacity of L-Arg-CS could be calculated to 3.12 mmol g^{-1} (198.2 mg g^{-1}), which is about 2.5 times as many as that of raw chitosan (shown in Table 1). The adsorption capacity of CS was greatly improved by modification of L-Arg. In comparison with other adsorbents reported in recent years [31,34–39], the adsorbent L-Arg-CS/Fe_3O_4 prepared in this work also showed higher adsorption capacity (shown in Table 1).

Table 4
The values of separation factor based on the Langmuir equation.

C_0	0.25	0.5	1.0	2.0	3.0	4.0	5.0	6.0	7.0	8.0
R_L	0.56	0.39	0.24	0.14	0.097	0.074	0.060	0.051	0.044	0.039

In order to study the adsorption behavior between L-Arg-CS/Fe_3O_4 and Cu(II) ions, Freundlich and Langmuir isotherm models were introduced to simulate the experiment data.

The Freundlich isotherm model assumes that the adsorption process occurs on energetically heterogeneous surfaces and adsorption capacity is related to the concentration of metal ion at equilibrium [47]. The Freundlich model can be expressed as:

$$\log Q_e = \log K_F + \frac{1}{n}\log C_e \tag{5}$$

where Q_e and C_e are the adsorption capacity (mmol g^{-1}) and the equilibrium concentration of Cu(II) (mmol L^{-1}), respectively; K_F (mmol g^{-1}) and n are Freundlich constant related to adsorption capacity and intensity. The experimental data were plotted as logQ_e versus logC_e (see Fig. 12a)

The Langmuir isotherm model predicts that a monolayer adsorption takes place without any interaction between the adsorbed molecules [48]. The equation of Langmuir isotherm is as follows:

$$\frac{C_e}{Q_e} = \frac{C_e}{Q_{max}} + \frac{1}{K_L Q_{max}} \tag{6}$$

where Q_{max} is the maximal absorption capacity (mmol g^{-1}) of adsorbent; K_L is Langmuir constant (L $mmol^{-1}$). The experimental data were plotted as C_e/Q_e versus C_e in order to evaluate the values of Q_{max} and K_L (see Fig. 12b).

The calculated constants and correlation coefficients values for Freundlich and Langmuir models are listed in Table 3. Compared with Freundlich model (R^2 = 0.90866), the Langmuir isotherm model fits better to the experimental data due to the higher correlation coefficients (R^2 = 0.99912). The maximum absorption capacity calculated by Langmuir model (2.25 mmol g^{-1}) fits well with the experimental maximum adsorption capacity (2.13 mmol g^{-1}). Based on the above facts, it can be deduced that the monolayer Langmuir adsorption isotherm is more reasonable to explain the adsorption behavior between L-Arg-CS/Fe_3O_4 and Cu(II).

Furthermore, the affinity between L-Arg-CS/Fe_3O_4 and Cu(II) can be predicted by the Langmuir parameter of the dimensionless separation factor R_L, which is defined by the following equation:

$$R_L = \frac{1}{1 + K_L C_0} \tag{7}$$

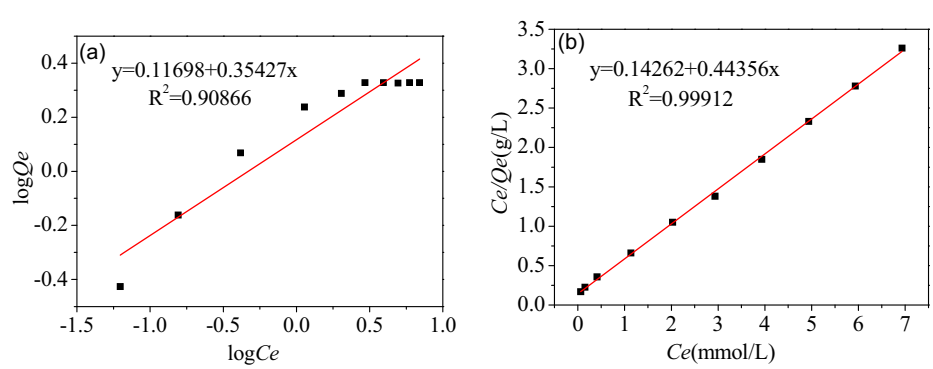

Fig. 12. The Freundlich (a) and Langmuir (b) adsorption isotherms.

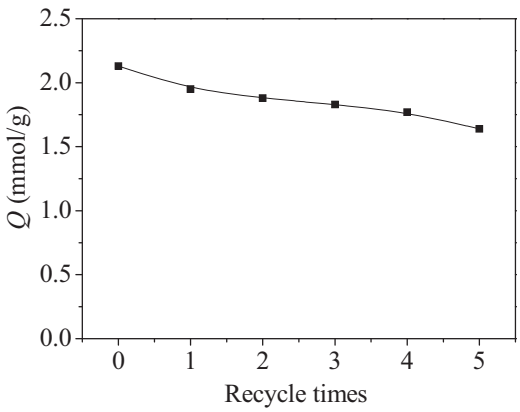

Fig. 13. Effects of regenerative times on the adsorption capacity.

where C_0 is initial concentration of Cu(II) (mmol L^{-1}); K_L is the affinity constant of Langmuir adsorption (L $mmol^{-1}$).

The value of R_L is always used to indicate whether the adsorption is favorable or not. $R_L > 1.0$, unfavorable; $R_L = 1.0$, linear; $0 < R_L < 1.0$, suitable and $R_L = 0$, irreversible [49,50]. The values of R_L calculated according to Eq. (7) are listed in Table 4. From Table 4, it can be seen that all of the R_L values are in the range of 0–1.0, indicating that the adsorption between L-Arg-CS/Fe_3O_4 and Cu(II) is favorable.

3.2.4. Regeneration and reuse of L-Arg-CS/Fe_3O_4

The investment cost of wastewater treatment is directly influenced by the regenerative performance of adsorbent. So five adsorption-desorption consecutive cycles were performed in order to evaluate the reuse possibility of L-Arg-CS/Fe_3O_4 for Cu(II) adsorption. As shown in Fig. 13, the regenerative L-Arg-CS/Fe_3O_4 still possessed high adsorption capability, which declined slightly with increasing cycle times. The adsorption capacity reduced to 1.64 mmol g^{-1} (about 77% of the initial value) after five times regeneration. It confirmed the good reusability and stability of the adsorbent.

3.3. Adsorption and desorption mechanism

L-Arg-CS/Fe_3O_4 have abundant active groups, such as amino, imino, carboxyl and hydroxyl, which can adsorb Cu(II) by coordination to form adsorbent-Cu(II) complexes on the surface of the adsorbent. By magnetic separation, Cu(II) ions were removed from aqueous solution. After separation, the adsorbent-Cu(II) complexes were placed into HCl solution, which supplied large amounts of H^+. Compared with Cu(II) ions, H^+ ions show stronger coordination ability due to the smaller radii. So Cu(II) ions were substituted by H^+ ions in adsorbent-Cu(II) complexes and Cu(II) ions returned to the solution. Finally, the L-Arg-CS/Fe_3O_4 adsorbent was regenerated after being stirred in NaOH solution and washed to neutralize. Therefore, above operations maintained the high adsorption capacity of L-Arg-CS/Fe_3O_4 in each cycle.

4. Conclusions

In this study, a new adsorbent L-Arg-CS/Fe_3O_4 was synthesized in order to adsorb Cu(II) in aqueous solution. The maximum adsorption capacity was confirmed as 2.13 mmol g^{-1} at pH = 5.5, t = 13 min and C_0 = 4.0 mmol L^{-1}. Kinetics study indicates that the adsorption behavior can be better described by the pseudo-second-order equation ($R^2 > 0.999$) and the rate-controlling step may be chemical adsorption. Adsorption isotherm simulation shows that Langmuir model fits better with the experimental data ($R^2 > 0.999$) than Freundlich model, implying the monolayer adsorption between the adsorbent and Cu(II). The values of separation factor ($0 < R_L < 1.0$) indicate that the adsorption is a favorable process. After adsorbing Cu(II), the adsorbent-Cu(II) complexes could be rapidly separated from aqueous solution by external magnetic field. The adsorbent still possessed excellent regenerative performance after five regenerative cycles. The results show that L-Arg-CS/Fe_3O_4 is a promising adsorbent for removal of Cu(II) from aqueous solutions.

Acknowledgements

This work was financially supported by the National Natural Science Foundation of China (Grant No. 21007029, 51472132), Qingdao Project of Science and Technology, China (Grant No. 13-1-4-114-jch), the Natural Science Foundation of Shandong Province, China (Grant No. ZR2012BQ017) and the Open Research Program of State Key Laboratory of Geological Processes and Mineral Resources, China (Grant No. GPMR201510).

References

[1] L.L. Fan, C.N. Luo, Z. Lv, F.G. Lu, H.M. Qiu, Colloids Surf. B 88 (2011) 574.
[2] G.M. Gadd, J. Chem. Technol. Biotechnol. 84 (2009) 13.
[3] J.L. Wang, C. Chen, Biotechnol. Adv. 27 (2009) 195.
[4] D. Jellouli Ennigrou, M. Ben Sik Ali, M. Dhahbi, Desalination 343 (2014) 82.
[5] M.R. Awual, M. Ismael, M.A. Khaleque, T. Yaita, J. Ind. Eng. Chem. 20 (4) (2014) 2332.
[6] Lalhmunsiama, S.M. Lee, D. Tiwari, Chem. Eng. J. 225 (2013) 128.
[7] L.L. Fan, C.N. Luo, Z. Lv, F.G. Lu, H.M. Qiu, J. Hazard. Mater. 194 (2011) 193.
[8] J.F. Liu, Z.S. Zhao, G.B. Jiang, Environ. Sci. Technol. 42 (2008) 6949.
[9] N.K. Lazaridis, G.Z. Kyzas, A.A. Vassiliou, D.N. Bikiaris, Langmuir 23 (2007) 7634.
[10] N.V. Majeti, R. Kumar, React. Funct. Polym. 46 (2000) 1.
[11] M. Rinaudo, Prog. Polym. Sci. 31 (2006) 603.
[12] H.Q. Bao, L. Li, L.H. Gan, Y. Ping, J. Li, P. Ravi, Macromolecules 43 (2010) 5679.
[13] X.Y. Li, H.H. Zhou, W.Q. Wu, S.D. Wei, Y. Xu, Y.F. Kuang, J. Colloid. Interface Sci. 448 (2015) 389.
[14] J.L. Wang, C. Chen, Biores. Technol. 160 (2014) 129.
[15] F.C. Wu, R.L. Tseng, R.S. Juang, J. Environ. Manage. 91 (2010) 798.
[16] D.H. Reddy, S.M. Lee, Adv. Colloid Interface Sci. 201–202 (2013) 68.
[17] P.A. Nishad, A. Bhaskarapillai, S. Velmurugan, S.V. Narasimhan, Carbohyd. Polym. 87 (2012) 2690.
[18] A. Ghaee, M. Shariaty-Niassar, J. Barzin, A. Zarghan, Appl. Surf. Sci. 258 (2012) 7732.
[19] S.P. Kuang, Z.Z. Wang, J. Liu, Z.C. Wu, J. Hazard. Mater. 260 (2013) 210.
[20] X.J. Hu, J.S. Wang, Y.G. Liu, X. Li, G.M. Zeng, Z.L. Bao, X.X. Zeng, A.W. Chen, F. Long, J. Hazard. Mater. 185 (2011) 306.
[21] Z.C. Wu, Z.Z. Wang, J. Liu, J.H. Yin, S.P. Kuang, Int. J. Biol. Macromol. 81 (2015) 838.
[22] L. Wang, R.G. Xing, S. Liu, Y.K. Qin, K.C. Li, H.H. Yu, R.F. Li, P.C. Li, Carbohydr. Polym. 81 (2010) 305.
[23] L.M. Zhou, J.H. Liu, Z.R. Liu, J. Hazard. Mater. 172 (2009) 439.
[24] Y.Z. Wen, J.Q. Ma, J. Chen, C.S. Shen, H. Li, Q.P. Liu, Chem. Eng. J. 259 (2015) 372.
[25] Y. Ren, H.A. Abbood, F.B. He, H. Peng, K.X. Huang, Chem. Eng. J. 226 (2013) 300.
[26] L. Tosi, A. Gamier, Biochem. Biophy. Res. Commun. 58 (1974) 427.
[27] M.T.L.S. Duarte, M.A.A. De, C.T. Carrondo, M.L.S. Goncalves, M.B. Hursthouse, N.P.C. Walker, H.M. Dawes, Inorg. Chim. Acta 124 (1986) 41.
[28] M. Monier, Int. J. Biol. Macromol. 50 (2012) 773.
[29] A.W. Chen, G.M. Zeng, G.Q. Chen, X.J. Hu, M. Yan, S. Guan, C. Shang, L.H. Lu, Z.J. Zou, G.X. Xie, Chem. Eng. J. 191 (2012) 85.
[30] L.M. Cui, L.H. Hu, X.Y. Guo, Y.K. Zhang, Y.G. Wang, Q. Wei, B. Du, J. Mol. Liq. 198 (2014) 157.
[31] Y.Y. Meng, D.Y. Chen, Y.T. Sun, D.L. Jiao, D.C. Zeng, Z.W. Liu, Appl. Surf. Sci. 324 (2015) 745.
[32] D. Hritcu, M.I. Popa, N. Popa, V. Badescu, V. Balan, Turk. J. Chem. 33 (2009) 785.
[33] H. Yan, L.Y. Yang, Z. Yang, H. Yang, A.M. Li, R.S. Cheng, J. Hazard. Mater 229–230 (2012) 371.
[34] W.S.W. Ngah, C.S. Endud, R. Mayanar, React. Funct. Polym. 50 (2002) 181.
[35] L.M. Zhou, Y.P. Wang, Z.R. Liu, Q.W. Huang, J. Hazard. Mater. 161 (2009) 995.
[36] Y.M. Ren, M.L. Zhang, D. Zhao, Desalination 228 (2008) 135.
[37] B. Kannamba, K.L. Reddy, B.V. AppaRao, J. Hazard. Mater. 175 (2010) 939.
[38] Y.H. Zhu, J. Hu, J.L. Wang, J. Hazard. Mater 221–222 (2012) 155.
[39] L.Q. Zhao, X.L. Chang, R. Liao, X.L. Zhang, J.R. Xie, B.W. Yu, R.H. Wu, R.J. Wang, S.T. Yang, Mater. Lett. 135 (2014) 154.
[40] S. Lagergren, Handlingar 24 (1898) 1–39.
[41] L.L. Li, C.N. Luo, X.J. Li, H.M. Duan, X.J. Wang, Int. J. Biol. Macromol. 66 (2014) 172.
[42] L.L. Fan, C.N. Luo, M. Sun, X.J. Li, H.M. Qiu, Colloids Surf. B 103 (2013) 523.

[43] M. Monier, D.M. Ayad, Y. Wei, A.A. Sarhan, J. Hazard. Mater. 177 (2010) 962.
[44] L.M. Zhou, C. Shang, Z.R. Liu, G.L. Huang, A.A. Adesina, J. Colloid. Interface Sci. 366 (2012) 165.
[45] K.Z. Elwakeel, A.A. Atia, J. Cleaner Prod. 70 (2014) 292.
[46] A.A. Atia, A.M. Donia, K.Z. Elwakeel, Hydrometallurgy 87 (2007) 197.
[47] Z. Zawani, C.A. Luqman, S.Y.C. Thomas, Eur. J. Sci. Res. 37 (2009) 63.
[48] Y.H. Li, Z. Di, J. Ding, D. Wu, Z. Luan, Y. Zhu, Water Res. 39 (2005) 605.
[49] Z. Aksu, Process Biochem. 38 (2002) 89.
[50] A.S. Alzaydien, W. Manasreh, Int. J. Phys. Sci. 4 (2009) 172.